Heliyon 10 (2024) e30116

Contents lists available at ScienceDirect

Heliyon

journal homepage: www.cell.com/heliyon

Research article

Synthesis of layered double hydroxides: Investigating the impact of stirring conditions and reactor design parameters

Rafaela Gabriel [a], Pollyanna Vanessa dos Santos Lins [a], Felipe de Alcântara Moura Vilela [b], Sandra Helena Vieira de Carvalho [c], Rodolfo Junqueira Brandão [b], João Inácio Soletti [c], Lucas Meili [a,*]

[a] Laboratory of Processes, Center of Technology, Federal University of Alagoas, Maceió, Alagoas, 57072-900, Brazil
[b] Flowlab, Center of Technology, Federal University of Alagoas, Maceió, Alagoas, 57072-900, Brazil
[c] Laboratory of Separation Systems and Optimization Processes, Center of Technology, Federal University of Alagoas, Maceió, Alagoas, 57072-900, Brazil

ARTICLE INFO

Keywords:
Process variables
Hydrotalcite
Structural characteristics

ABSTRACT

The synthesis by coprecipitation of Layered Double Hydroxides (LDHs) is governed by the stages of nucleation and crystal growth associated with the efficiency of the mixing and dispersion process of the reagents. Mixing efficiency is related to process variables, such as agitation speed, type of impeller and baffles presence, among others. In this context, this work proposes an analysis of these variables in a batch reactor, using a 2^3 factorial design employing the factors: acceleration speed (200 and 1000 rpm), mixing time (2 and 18 h) and presence or absence of baffles. The results were evaluated quantitatively (amount of LDH produced, time and amount of base for the formation of LDHs to begin) and qualitatively (mixing aspects, sedimentation ad grinding). The significant factors affecting the amount of LDH produced (51.94–80.81 g) were agitation speed and aging time. These factors were also correlated with the structural characteristics of the materials produced, such as crystallinity, crystallite size (70.99–174.79 nm), surface area (69.81–97.62 m^2/g), pore volume (0.28–0.59 cm^3/g), and pore diameter (11.40–34.66 nm). LDHs produced at higher agitation rates (1000 rpm) and longer aging times (18 h) yielded higher quantities of materials (80.81 g) with improved structural characteristics. The study highlights the importance of systematically exploring the synergistic effect between process variables, emphasizing the research potential in this area.

1. Introduction

The term Layered Double Hydroxide (LDH) refers to a class of inorganic lamellar compounds of basic character and high capacity to intercalate anions. A wide variety of LDHs can be synthesized from a wide combination of metal cations (Mg^{2+}, Ni^{2+}, Fe^{2+}, Zn^{2+}, Al^{3+}) and interlayer anions (CO_3^{2-}, OH^-, F^-, Cl^-, Br^-, NO^{3-}, I^-) [1–3]

In the preparation of LDHs, a factor of great importance is the stabilization of the lamellar structure, which is possible due to electrostatic attraction forces existing between the lamellae (positive force) and the interlamellar anions (negative force). Therefore, the ratio of M^{2+}/M^{3+} defines the density of the lamellar charge and consequently the number of anions between the lamellae. This

* Corresponding author.
E-mail address: lucas.meili@ctec.ufal.br (L. Meili).

https://doi.org/10.1016/j.heliyon.2024.e30116
Received 8 January 2024; Received in revised form 26 March 2024; Accepted 19 April 2024
Available online 20 April 2024

relationship has a significant impact on the physical and chemical properties of the material, such as crystallinity, porosity, surface area, and ion exchange capacity. The definitions of these characteristics are also associated with the synthesis process, as the process strongly depends on the degree of homogeneity obtained during the mixing stage of the reagents, while promoting nucleation and crystal growth [4–6]

Therefore, standardization of reaction conditions (chemical and process variables) is crucial to improve the efficiency of the agitation and mixing process, which are related to mass transfer phenomena and energy transmitted to the system to enhance the degree of dispersion between particles in a solid-liquid mixture [7–9]

Regarding the effects of chemical variables, the specific literature points out that the synthesis process suffers the effects of chemical variables, such as: proportions of trivalent and divalent cations, stirring time, temperature and reaction time, thus, there are several works aimed at determining these factors in the literature, such as the works of Ahmed et al. [10]; Elhalil et al. [11]; Valente et al. [12]; Yuan et al. [13] and Zou et al. [14].

On the other hand, the effects of the influence of process variables on the structural characteristics of LDHs have not yet been fully elucidated. This stage involves the selection of operational conditions, such as: agitation speed, types of impellers, impeller clearance, baffles, baffle width, among others [15].

The studies conducted by Sun et al. [16] already signaled the need to expand the study of reaction conditions by including other parameters, such as agitation rate and reagent addition rate. A literature search on process variables applied to the synthesis of LDHs identified some works that mention agitation rates (rpm) and reagent addition rates (mL/min): 200 rpm [17,18], 400 rpm [19], 700 rpm [20], 1200 rpm [21], 1300 rpm and 7.5 mL/min [22], 1400 rpm [23], 1 mL/min [24,25], 60 mL/min [26] and 4 mL/min [27,28]. However, in these works, the effects of these factors on LDH synthesis were not evaluated.

Therefore, it is imperative to complement the missing information in the literature regarding the structuring part of the batch reactor for LDH synthesis. It is believed that process variables, as well as chemical variables, can justify the structural and morphological characteristics of LDHs, based on theoretical criteria of the agitation and mixing effect of the reaction fluid.

In this context, this work provides an assessment of the influence of stirring speed (200 and 1000 rpm), stirring time (2 and 18 h) and presence or absence of baffles in the production process and formation of LDHs synthesized by the coprecipitation method at variable pH, with the response being the variation in the amount of produced LDH (dry mass) evaluated through a 2^3 factorial design. Furthermore, the results were correlated with aspects of the reaction mixture observed during the experiments and the changes in the physical-chemical characteristics of the materials, assessed through characterization techniques including X-Ray Diffraction (XRD), Thermogravimetric Analysis (TGA/DTG), Fourier Transform Infrared Spectroscopy (FT-IR), and Nitrogen Adsorption using the Brunauer, Emmett, and Teller (BET) and Barrett-Joyner-Halenda (BJH) methods, which demonstrate a good interaction with the process variables.

2. Materials and methods

2.1. Synthesis of LDHs

To evaluate the influence of process variables on LDH syntheses, a complete 2^3 factorial design was used, the number "2″ indicates the number of levels evaluated, while the number "3″ indicates the number of factors studied in the experiment, o número de variávies, resulting in 8 experiments. The variables investigated and their respective levels were a) agitation speed: 200 and 1000 rpm; b) mixing time: 2 and 18 h and c) presence/absence of baffles, as set out in Table 1. In the symbolism used, HTnc, HT represents the name hydrotalcite corresponding to the LDHs produced with Mg and Al, *n* corresponds to the trial number and *c* represents the presence of baffles. To generate the coded matrix, the STATISTICA 12 Software was used as support. The rotation speeds and mixing time (aging time) were defined based on the reactor's safety limits and LDH production data used in previous studies: Cermelj et al. [20]; Di Cosimo et al. [29]; Modrogan et al. [17]; Teixeira et al. [18]; Thite & Giripunje [21].

To conduct the syntheses, the reaction conditions were chosen based on the selection of chemical variables (fixed) and process variables. LDHs were synthesized by the coprecipitation method at variable pH based on and adapapted from studies developed by Ref. [30–32]. LDHs were produced in a 2:1 Mg/Al ratio using two solutions; a solution A, containing $Mg(NO_3)_2.6H_2O$ 1.42 M and Al $(NO_3)_3.9H_2O$ 0.71 M in 434 mL of deionized water and a solution B composed of NaOH 2.2 M and Na_2CO_3 1.2 M in 700 mL of deionized

Table 1
Planning variables and levels $2.^3$.

	LDH	Planning variables		
		Speeds (rpm)	Time (h)	Baffles
1	**HT1**	200 (−1)	2 (−1)	Without baffles (−1)
2	**HT2**	1000 (1)	2 (−1)	Without baffles (−1)
3	**HT3**	200 (−1)	18 (1)	Without baffles (−1)
4	**HT4**	1000 (1)	18 (1)	Without baffles (−1)
5	**HT5c**	200 (−1)	2 (−1)	With baffles (1)
6	**HT6c**	1000 (1)	2 (−1)	With baffles (1)
7	**HT7c**	200 (−1)	18 (1)	With baffles (1)
8	**HT8c**	1000 (1)	18 (1)	With baffles (1)

water.

Initially, solution B was dripped onto solution A with the aid of a peristaltic pump at a constant rate of 15 mL/min at room temperature and variable speed (200 and 1000 rpm) according to Table 1. The pH of the final solution after addition of solution B it was equal to 12.

The syntheses of MgAl-LDH were conducted in a pilot unit consisting of a 1.5 L jacketed reactor for water circulation, coupled with a temperature (thermostatic bath) and speed (mechanical stirrer) control system. The reactor is integrated with inlets for adding pH and temperature control reagents that allow direct contact with the reaction medium, while the reactor's internal system consists of baffles and impellers. In the present study, the type of impeller used was pitched blades. Fig. 1 shows the main control components and auxiliary equipment that make up the internal structure of the reactor integrated with auxiliary equipment. The characteristics of the auxiliary equipment that controls the main process variables are specified in Table 2.

After the precipitation step, the aging temperature was adjusted to 60 °C for a variable time (2 and 18 h), as shown in Table 1. After the synthesis step, colloidal solutions of dispersed LDHs in a liquid phase were obtained, forming LDH gels with a viscous appearance. The gels underwent the following subsequent steps: a) washing, conducted in a centrifuge with 5 repetition cycles at 2500 rpm; b) drying, carried out in an oven at 105 °C for 4 h and c) maceration and sieving, to obtain LDHs in powder form with a size smaller than 0.425 mm. As responses to the planning, the amount of MgAl-LDH (m_{LDH}) produced, qualitative aspects of the mixture and characteristics of the LDHs formed were evaluated. The LDH mass was obtained by weighing on an analytical balance.

2.2. Image analysis

For each stirring speed (200, 600 and 1000 rpm), a video was recorded, and 11 frames were taken from each video for analysis. Using ImageJ software, the original frame underwent the following changes: conversion to 8-bit grayscale images, improvement of image contrast and creation of regions of interest (RoI). The RoIs were positioned in such a way that they represented significant areas for analysis, avoiding regions of high reflection and distortion due to the curvature of the container.

In each RoI, the average of the pixel's gray value was calculated (Equation (1)), the standard deviation of the pixel's gray value (Equation (2)), then the coefficient of variation (CV) was obtained (Equation (3)), and the average of these values between the replicas, obtaining a characteristic frame for each speed. Then, the mean and standard deviation of the CV between the RoIs of each characteristic condition were calculated.

$$\dot{C} = \frac{\sum_{i=1}^{m} C_i}{m-1} \tag{1}$$

$$\sigma = \sqrt{\frac{\sum_{i=1}^{m} (C_i - \dot{C})^2}{m-1}} \tag{2}$$

$$CV = \frac{\sigma}{\dot{C}}\, x\, 100\% \tag{3}$$

Where σ is the standard deviation of the gray value, $\dot{C}$ is the mean gray value, and m is the number of pixel points in the samples.

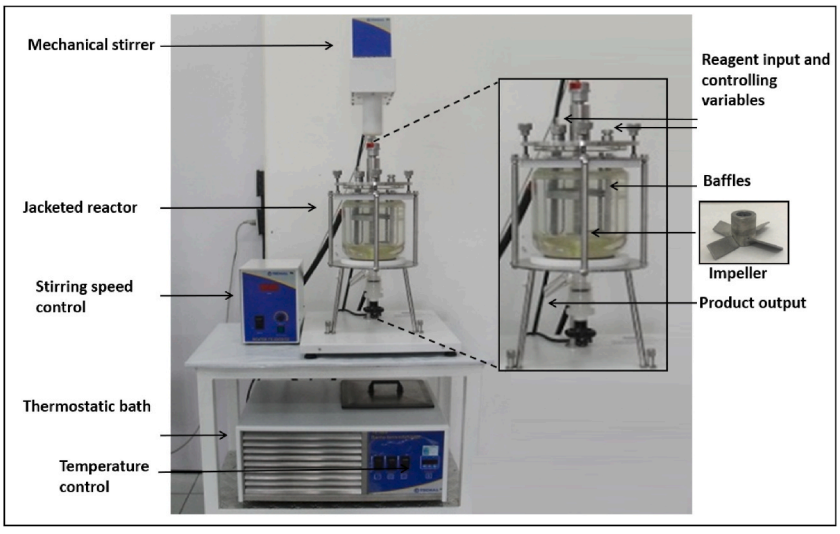

Fig. 1. Pilot unit used to produce LDHs.

Table 2
Specifications of auxiliary equipment.

Equipment	Specifications	Controlled variable
Thermostatic bath	Model TE–184, TECNAL	Water temperature
Digital thermometer	Model K29-5030, KASVIN	Mixture temperature
Peristaltic pump	Watson Marlon brand	Reagent flow
pH meter	Model TEC-7, TECNAL	pH of the mixture

2.3. Characterization of LDHs

XRD analyzes were performed on a 7000 SHIMADZU diffractometer using Cu radiation ($\lambda = 0.154060$ nm) at 40 kV and 30 mA. The patterns were recorded in a range of range from 3 to 70°, in increments of 0.02°.

The basal spacings, cell parameter (a and c) and particles size were calculated for each material. Basal spacings were determined according to equation (4), Bragg's Law and the cell parameter with Equations (5) and (6) [6], respectively:

$$n\lambda = 2d_{hkl}Sen\theta \tag{4}$$

$$a = 2d_{110} \tag{5}$$

$$c = \frac{3}{2}(d_{003} + 2d_{006}) \tag{6}$$

Where n is the peak reflection order ($n = 1$), λ is the X-ray wavelength used in the analysis, d is the basal spacing for the hkl peak and θ is the Bragg angle determined by the diffraction peak.

The average particles size was determined by the Scherrer equation [33], according to Equation (7):

$$D = \frac{k\lambda}{\beta \cos(\theta_B)} \tag{7}$$

Where, k represents the shape factor, λ the wavelength of k-αCu radiation, $\boldsymbol{\beta}$ is width at half height of the diffraction peak (FWHM) and $\boldsymbol{\theta_B}$ is the Bragg angle.

Thermogravimetric analyzes were carried out using a Shimadzu thermobalance, model SDT650. Around 10 mg of the sample was placed in alumina crucibles and subjected to temperatures up to 900 °C at a heating rate of 10 °C.min^{-1}, in a synthetic air atmosphere

Table 3
Design of experiments matrix 2^3 and synthesis of quantitative and qualitative results.

LDH	Process variables	Quantitative results			Qualitative results		
		Formation of LDHs		Amount of LDH produced (g)	Aspects of the mixture	Washing and sedimentation[a]	Aspects of crushing
		Time (min)	$V_{solution\ A}$ (mL)				
HT1	200 rpm/2h	25	250	51.94	Pasty liquid and presence of agglomerated reagent mass.	Easy washing due to the fast sedimentation of the LDHs. (5 min)	LDH is difficult to crush.
HT2	1000 rpm/2h	18	180	77.42	Uniform pasty gel.	Hard washing due to slow sedimentation of the LDHs (7 min)	LDH is easy to crush.
HT3	200 rpm/18h	25	250	63.00	Pasty gel with the presence of an agglomerated reagent mass and liquid part at the base of the reactor.	Easy washing due to the fast sedimentation of the LDHs. (5 min)	LDH is difficult to crush.
HT4	1000 rpm/18h	18	180	73.99	Uniform pasty gel with high apparent viscosity.	Hard washing due to slow sedimentation of the LDHs (7 min)	LDH is easy to crush.
HT5c	200 rpm/2h/baffle	20	200	52.08	Pasty gel with the presence of an agglomerated reagent mass and liquid part at the base of the reactor.	Easy washing due to the fast sedimentation of the LDHs. (4min)	LDH is difficult to crush.
HT6c	1000 rpm/2h/baffle	16	160	70.42	Uniform pasty liquid.	Easy washing due to the fast sedimentation of the LDHs. (5 min)	LDH is easy to crush.
HT7c	200 rpm/18h/baffle	20	200	64.96	Pasty gel with the presence of an agglomerated reagent mass.	Easy washing due to the fast sedimentation of the LDHs. (4min)	LDH is difficult to crush.
HT8c	1000 rpm/18h/baffle	16	160	80.81	Uniform pasty liquid.	Moderate ease of washing due to sedimentation (6 min)	LDH is easy to crush.

[a] The sedimentation ease was evaluated by the sedimentation time (min) of the LDH particles and by the transparency of the washing water.

with a flow rate of 50 mL min^{-1}.

The FT-IR spectra were obtained on a Shimadzu IRTracer-100 equipment in the region of 4000 to 400 cm^{-1} with a resolution of 4 cm^{-1} using the KBr pellet technique. The tablets were prepared by pressing using 0.5–1% by mass of sample in relation to the mass of KBr to ensure detection of the bands.

Nitrogen adsorption tests were performed using an automated gas sorption analyzer, Quantachrome instruments, NOVA 4200e, USA. Each sample was treated at 300 °C for 12 h. And after treatment, the samples were subjected to a flow of nitrogen gas at −196 °C. The specific surface area was obtained using the Brunauer, Emmett, Teller (BET) method and the pore size distribution using the Barrett-Joyner-Halenda (BJH) method.

3. Results and discussion

In this session, the main operational parameters of a batch reactor for the synthesis of MgAl-LDH prepared by the variable pH coprecipitation method were examined. The data obtained was collected in Table 3 and divided into quantitative and qualitative results.

3.1. Quantitative analysis

In this session, the influence of process variables (speed, time and baffles) on the formation of LDH and the quantity (m_{LDH}) produced in each test was discussed. The information was obtained in Tables 3 and in the section on quantitative data.

The first aspect analyzed reflects the change in apparent viscosity of the reaction medium. The viscosity alteration occurred during the precipitation step, wherein the reaction mixture underwent a drastic change in appearance upon addition of solution A (NaOH and Na_2CO_3). At this point it was attributed that the structural formation of LDHs occurred more intensely, marked by a drastic change in viscosity. The amount of base (mL) and time were recorded for comparison between mixtures.

The data demonstrated that all LDHs produced at a speed equal to 1000 rpm had shorter times (16–18 min) until the effective formation of LDHs, while systems stirred at 200 rpm were slower (20–25 min); also implying an increase in the amount of base used (160 mL–250 mL). It is also noteworthy that the presence of baffles in the reaction medium favored the effective formation of LDHs, since shorter times and smaller amounts of base were required in the presence of baffles.

At 1000 rpm, the use of the baffle reduced the time until the intense formation of LDHs from 18 min to 16 min and the amount of base from 180 mL to 160 mL. The same behavior was observed at 200 rpm, where the time decreased from 25 to 20 min; and the amount of base, from 250 to 200 mL. This behavior suggests that there was better homogenization between the metal (solution A) and basic (solution B) solutions in the presence of baffles, leading to an accelerated formation of LDHs. Thus, it is evident that the use of the baffle favored the mixing process in the precipitation stage.

Another quantitative aspect analyzed was the influence of process variables on the amount of LDH produced. Table 4 presents the estimated effect data (main and interaction) after statistical treatment [34]. The Pareto chart, presented in Fig. 2, was constructed to help observe the variables that most influenced the results, within the statistical parameters studied.

The Pareto chart provided the direct results of the significance of the factors where the standardized effects were displayed in horizontal bars representing the tabulated t value. The results demonstrated that the significant factors having as a response the amount of LDH (m_{LDH}) were agitation speed and aging time. It is also observed that among the variables studied, the stirring speed was the dominant variable in terms of the amount of MgAl-LDH produced. The other factors, such as the presence or absence of chicanes and the second and third order interaction effects, did not show evidence of significance for the investigated study range, considering 95 % confidence.

Analyzing the agreement of the factorial design with the data obtained in Tables 3 and it is possible to relate the influence of significant factors on the amount of LDH produced (m_{LDH}). In tests 1 and 2, for example, when the speed increased from 200 to 1000 rpm, keeping the time constant, the amount of LDH produced also increased. The same behavior was observed in all other pairs with constant time: 3 and 4, 5 and 6 and 7 and 8. Furthermore, in trials 1 and 3, 5 and 7 and 6 and 8, in which the time of aging varied from 2 to 18 h, with constant speeds, the amount of LDH produced also increased.

These results are in accordance with the Pareto chart (Fig. 2) since the statistical analysis showed that the increase in speed and aging time favored the production of LDHs. However, in trials 2 and 4 the effect was reversed. This fact may be associated with the greater shear stress caused by the absence of a baffle and the high speed used in the test, which may have accelerated the fluid velocity and caused the material to become unstructured.

Table 4
Estimation of effects based on quantity of LDH (m_{LDH}) after statistical treatment ($R^2 = 0.9769$).

Factor	Effect estimation (%)	Standard error	T_3	Value p	Interval Estimation	
					Inferior limit (−95 %)	Upper limit (+95 %)
Average	66.83	0.89	74.89	0.00	63.99	69.67
Speed (S)	17.67	1.78	9.90	0.00	11.99	23.34
Time (T)	7,73	1.78	4,33	0.02	2.05	13.40
Speed x Time	−4.25	1.78	−2.38	0.10	−9.92	1.43
Time x Baffle	3.91	1.78	2.19	0.12	−1.77	9.59

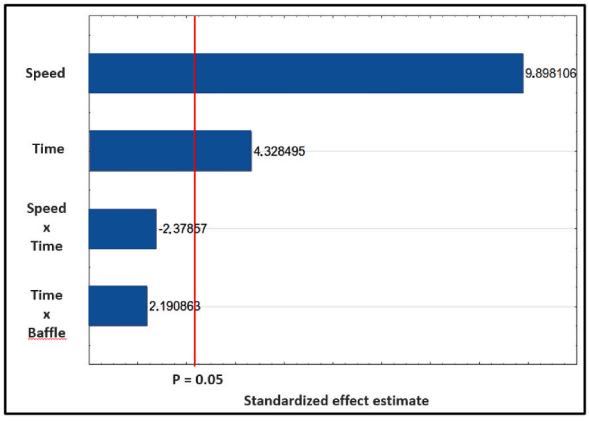

Fig. 2. Analysis of significant factors through a Pareto chart.

3.2. Qualitative analysis

In this session, the main changes noticeable in the mixing tank during the precipitation and aging stages were gathered, considering the homogeneity of the reaction medium; and also, observations during the washing and crushing stage, until the final obtaining of LDHs in powder form.

Fig. 3 shows the effects of stirring speed on LDHs production at the beginning of the precipitation phase (5 min). This point was chosen because it allowed a better evaluation of the characteristics of the mixtures, such as observation of flow characteristics and miscibility between reactants. The results captured demonstrated that when the speed increased, the reaction medium became more homogeneous. It is possible to observe that when the stirring speed is equal to 200 rpm the formation of undissolved portions of the basic solution occurred when this solution was precipitated over the metal solution (Fig. 3a). Hence, initially, one notices the agglomeration of those portions that were not instantly dissolved due to the low speed utilized in the synthesis process. On the other hand, with an increase in speed to 1000 rpm, the basic solution when inserted into the reactor dissolves quickly, forming a more homogeneous mixture than at 200 rpm and predominantly whitish, without the observation of empty spaces. (Fig. 3b). It is believed that this difference in homogeneity in the precipitation stage may have affected the nucleation stage of the LDHs, since, in a scenario of poor dispersion between the reactants, the nucleation stage is later [35].

In the precipitation stage, it was also possible to evaluate the influence between the use of baffles and the dissolution of the reagents. It was noticed that when using baffles, regardless of the speed used, the presence of undissolved portions of the basic solution precipitated over the metal solution was not observed. There was also a region of greater turbulence when the speed was adjusted to 1000 rpm. This demonstrates an improvement in the agitation process with the use of a baffle in the precipitation stage (comparison

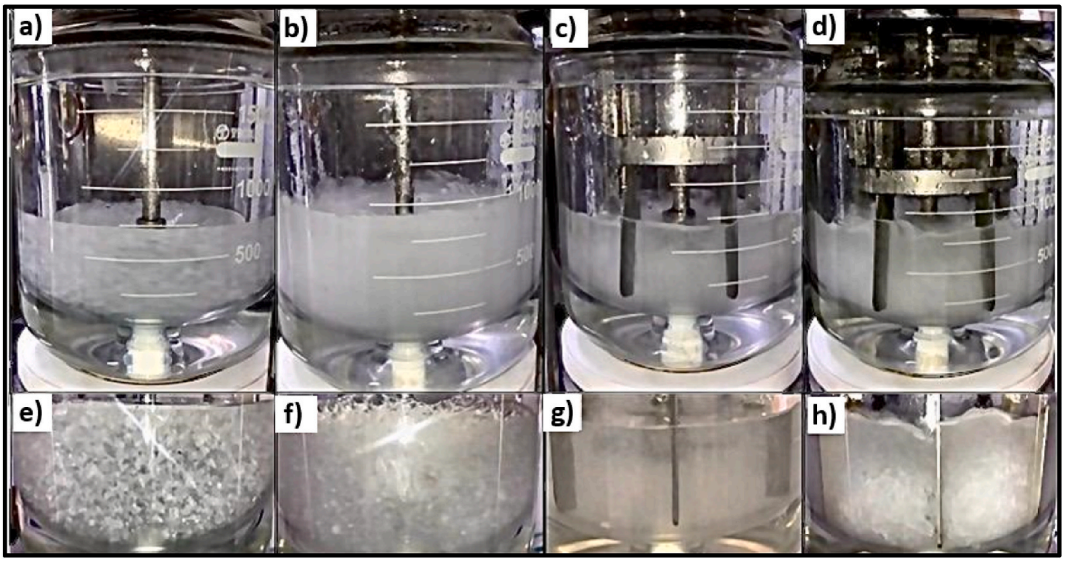

Fig. 3. Influence of rotation speed and presence of baffles on LDH formation, factors employed: a) 200 rpm, b) 1000 rpm, c) 200 rpm with baffle, d) 1000 rpm with baffle, e) 200 rpm, f) 1000 rpm, g) 200 rpm with baffle, and h) 1000 rpm with baffle.

between Fig. 3c and d). Fig. 3e–h are enlargements of Fig. 3a–h.

Thus, the experimental results demonstrated that the homogeneity of the LDH mixtures increased with the increase in the degree of agitation (considering the same mixing time) and that the presence of baffles at the beginning of the reaction has a positive impact on the flow profile within the reactor, evidenced by the absence of stagnant zones, regions of low homogeneity and solid body rotation (vortex formation).

Another factor analyzed was the aging time, which is the stage responsible for the growth of crystals and improving the crystallinity of the particles formed [6]. The influence of aging time on the production of MgAl-LDH LDHs can be explained in terms of the classical theory of crystal nucleation and growth.

For study purposes, the LDHs HT1 and HT3, stirred at 200 rpm, were chosen to represent the physical phenomena that occur inside the reactor over time. Fig. 4a–c exemplify the precipitation step with a fixed duration of 90 min for all tests. Initially, there was agglomeration of the basic precipitating solution caused by the deficiency in the miscibility of the phases due to the low stirring speed.

Over time, the agglomerated base portions were dissolved, and the stages of nucleation and growth of the crystals began to occur more intensely, marked by a visual change in the viscosity of the medium, where the reaction medium becomes composed of a viscous, whitish gel (Fig. 4c). At this stage, movements on the reactor walls are imperceptible due to the high viscosity and the intensity of the white color of the mixture. The time and volume spent from baseline to this point were recorded in Table 3.

After the precipitation stage, the aging stage began. It is worth noting that the tests have the same process parameters (200 rpm, without baffle), but different aging times, 2 h (Figs. 4d) and 18 h (Fig. 4e). Experimental observations indicated changes in viscosity with the evolution of aging time. On the surface of the reaction fluid in the stage represented by Fig. 4d, it is possible to perceive a more intense movement, with the fluid constantly rising and falling as it is stirred for 2 h, indicating a lower apparent viscosity than the fluid stirred for 18 h (Fig. 4e), which showed discrete movement on the surface of the mixture.

Generalizing the effects of aging time to the other tests, it was found that in all tests there was an increase in the apparent viscosity of the reactional medium, regardless of the time and the presence of baffles. However, tests conducted at low speed (200 rpm) showed poor mixing after completion of the total synthesis time. The presence of an agglomerated reagent mass was observed, forming a gel with a grainy appearance (Fig. 5a). On the other hand, in tests conducted at 1000 rpm, the final mixture formed a pasty gel with a uniform appearance, without the presence of agglomerated portions (Fig. 5b).

These differences in the materials formed interfered with the subsequent stage of sedimentation and crushing of the LDH crystals. These results were analyzed qualitatively and reflect changes in the ease of sedimentation and crushing of MgAl-LDH particles, which were associated with differences in weight and hardness between the particles.

According to Table 3, materials HT1, HT3, HT5c, HT6c and HT7c showed easy sedimentation in the washing stage. The ease of sedimentation was associated with the weight of the crystals, as heavier materials settle more easily and take less time. Therefore, these materials were given greater weight. Thus, the materials considered heavier, for the most part, had a lower agitation speed (200 rpm) in common, under conditions of varying aging time and use of baffles. At the other extreme, the opposite occurred, the crystals sedimented more slowly (HT2 and HT4) at higher agitation rates (1000 rpm). Thus, in general, it can be inferred that lighter crystals were produced at the higher speed level. As for the crushing stage, all tests conducted at 200 rpm (HT1, HT3, HT5c and HT7c) produced harder and more difficult to crush crystals. In general, it is observed that heavier materials form harder solids that are difficult to crush. These differences in the handling of materials are associated with process variables since the conditions of the chemical reaction were kept fixed during all experiments.

3.3. Characterization

The structural modifications of the LDHs produced in each reaction condition were also analyzed using instrumental techniques that allowed evaluating how process variables influenced the structural and morphological characteristics of the material, such as crystallinity, particle size, surface area and composition (appearance of undesirable phases).

The powder X-ray Diffraction (XRD) technique was used to identify the lattice parameters, crystallinity, and particles size of the MgAl-LDH samples produced in the reactor according to the process variables. Fig. 6 shows the arrangement and characteristics of the

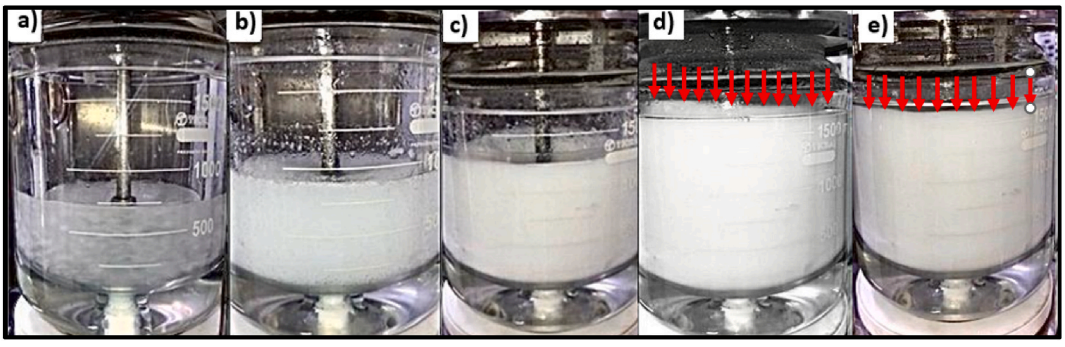

Fig. 4. Influence of mixing time on the production of MgAl-LDHs.

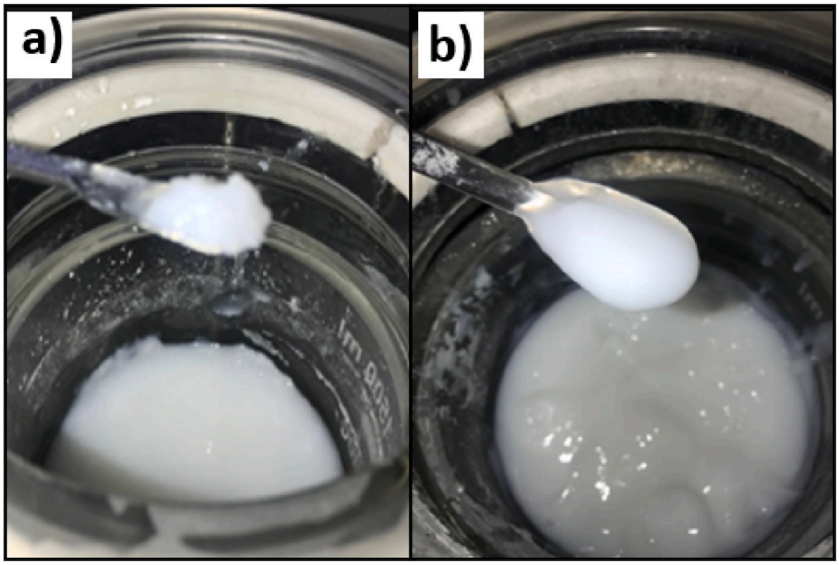

Fig. 5. Aspects of MgAl-LDH LDHs at the end of the synthesis time.

peaks. Table 5 shows the relationship between the crystalline planes, such as the lattice parameters and the particles size obtained for all the materials produced. Through the analysis of diffraction peaks, it was possible to confirm the formation of MgAl-LDHs based on the presence of diffraction planes characteristic of hydrotalcites, which presented symmetrical reflections for the planes (003), (006), (110) and (113), and the asymmetric reflections for the non-basal planes (012), (015) and (018).

It can be seen from Fig. 6 that the peak profiles present differences between them, with changes in height and width, these differences are indicative of the variation in the crystalline structure between the materials. The presence of narrow and intense peaks suggests that the hydroxides were synthesized with a high degree of crystallization and the symmetry and relative sharpness of the reflections indicate the absence of stacking faults.

The results in Table 5 confirmed the formation of LDHs in all tests and provide numerical data that allowed evaluating the difference between the particles produced. The calculated values for lattice parameters (a and c) and basal spacings (d_{003} and d_{006}) indicated the formation of a 3-R type crystalline arrangement (rhomboetric symmetry). Table 5 also provided an estimate of the particles size, with values between 70.99 and 174.79 nm.

Comparing the results obtained with the influence of stirring speed, it was found that tests HT2, HT4, HT6c and HT8c, conducted at higher stirring speeds (1000 rpm), presented the highest values for particle size, with values between 138.57 and 174.79 nm. While tests HT1, HT3, HT5c and HT7c, conducted at 200 rpm, showed smaller sizes, 70.99 and 113.01 nm. This behavior suggests that the agitation speed used in each test influenced the determination of the particle size of the produced LDHs.

Regarding the influence of aging time, it was found that increasing the aging time, from 2h to 18h, favored the growth process of

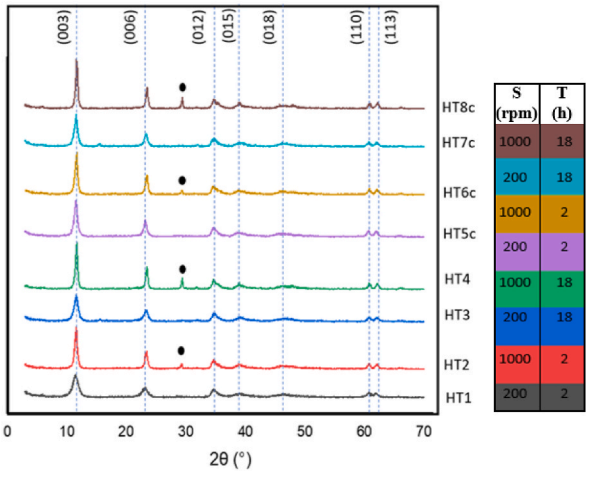

Fig. 6. X-ray diffraction diagram of the LDHs compounds produced.

Table 5
X-ray diffraction data.

LDH	Process variables	Basal Spacing (Å)		Cell Parameter (Å)		Particles size (nm)
		d_{003}	d_{006}	*a*	*c*	
HT1	200 rpm/2h	7.69	3.84	3.05	23.04	113.01
HT2	1000 rpm/2h	7.66	3.81	3.05	22.92	138.57
HT3	200 rpm/18h	7.65	3.82	3.04	22.93	92.33
HT4	1000 rpm/18h	7.61	3.79	3.04	22.79	172.85
HT5c	200 rpm/2h/baffle	7.73	3.85	3.00	23.14	70.99
HT6c	1000 rpm/2h/baffle	7.63	3.80	3.04	22.84	140.99
HT7c	200 rpm/18h/baffle	7.68	3.82	3.05	22.96	107.03
HT8c	1000 rpm/18h/baffle	7.59	3.79	3.04	22.75	174.79

LDHs crystallites. The evolution of the crystal with aging time was already expected, since data from the literature report that aging time leads to crystal growth [6]. However, in tests conducted at low-speed rates, it was not possible to establish a regular behavior of the variation in crystal size with stirring time. In this case, it is suggested that the stirring speed used (200 rpm) did not act efficiently in the mixing process and was not sufficient to cause adequate dispersion between reagents, which may have caused a disorderly variation in the size of the crystallite. These agree with the results observed in Fig. 5, where it was observed that the final appearance of the LDHs did not correspond to the appearance of a completely homogeneous mixture.

It is also worth highlighting the appearance of an atypical phase (●) highlighted in the diffractograms in Fig. 6, which appears at 2θ (degrees) = 29.4 and was attributed to the nitratin phase ($NaNO_3$), which may be associated with a phase not removed during washing [6,36]. It is also noted that all materials produced at 1000 rpm presented the nitratin phase. and that these materials showed better response in terms of the amount of LDH produced (51.94–80.81 g).

The other structural parameters, *a*, *c*, d_{003} and d_{006}, which appear in Table 5, suffered small variations, but did not present any pattern of behavior with the process variables. This result was already expected, since these parameters are influenced by the nature of the lamella cations and interlamellar anions, which in this study were kept fixed [37].

Thermogravimetric analyzes (TGA) and its derived curve (DTG) were used to evaluate the mass decomposition rate of LDHs produced as temperature increased. Fig. 7 presents the TGA curves and their respective DTG for all materials produced. Table 6 presents the main regions of mass losses (%) of the samples produced.

According to the analysis of Fig. 7, there are predominantly two well-defined regions of mass loss, in agreement with data reported in the literature that relate this behavior to hydrotalcites in the form of carbonate (Pérez et al., 2004b; [38]).

The first mass loss is in the range of 194–204 °C and is the result of the removal of water found in the interlayer space. In this region, mass losses varied from 11.03 to 17.77 % according to Table 6. The second region, which comprises the temperature range from 313 to 369 °C, can be related to the dehydroxylation and decarbonation steps that lead to decomposition and collapse of the structure of LDHs that give rise to oxides (Pérez et al., 2004b). In this region, the greatest mass losses were recorded, ranging from 21.71 to 24.83 %. It is also worth noting that these two stages may overlap in the curves.

It is further observed that other endothermic bands are noted, which may be related to the reabsorption of water on the material surface (●) [6] and the formation of magnesite and/or hydromagnesite phases (▲) [39]. The presence of these compounds, for the most part, was identified in tests conducted at 1000 rpm, regardless of the aging time and the presence of baffles. As already discussed, high speed increases the homogeneity of the mixture, but can also cause the material to become unstructured due to the increase in shear stress. These factors may have contributed to the formation of phases/compounds different from the typical phases/compounds of LDHs.

Spectroscopy in the Fourier Transform Infrared (FT-IR) region was used to identify the typical absorption bands of LDHs, providing evidence regarding the presence of functional groups that characterize a sample (J. [40]). Fig. 8 shows the main absorption bands of the LDH samples (HT1-HT8c). Through analysis of the FT-IR spectra, it was verified that the samples presented, for the most part, bands characteristic of hydrotalcite-type materials [41]. The bands located between 3400 and 3500 cm^{-1} are attributed to the vibrations of the O–H groups present between the layers in interlayer water molecules [42,43]. The region close to 1600 cm^{-1} may be associated with the angular stretching of water molecules between the lamellae or water of hydration. While the bands 1377 and 1067 cm^{-1} may indicate the presence of asymmetric stretching of CO_3^{2-} ions, present due to the contact of LDHs with the atmosphere [44]. The bands between 500 and 900 cm^{-1} indicate metal-oxygen (M − O) vibrations of the bonds between cations and oxygen. More specifically, these bands correspond to stretching vibrations of the Al–O or Mg–O band that represent the characteristic spectrum of LDHs according to the metals used in their production [45].

Additionally, Fig. 8 depicts alterations in the intensity of bands. In most tests conducted in the presence of baffles, characteristic bands of lower O–H group vibrations were observed, suggesting that the presence of interlayer water molecules varied with the process conditions used in LDH production. These results, in general, are also consistent with the mass loss data obtained from TGA/DTG (Table 6), which showed variation in the removal of water from the interlayer space (11.53–17.77 %), the variation of which relates to the estimation of the minimum chemical composition of the samples. (Pérez et al., 2004). The remaining bands showed minor intensity alterations. Nevertheless, it can also be inferred that there was a change in the typical functional groups of LDHs with process conditions, even starting from a fixed ratio of reagents. As suggested earlier, process variables alter the homogeneity of the reaction medium, which can lead to changes in connectivity between reactants and consequent compositional variation. The changes in the

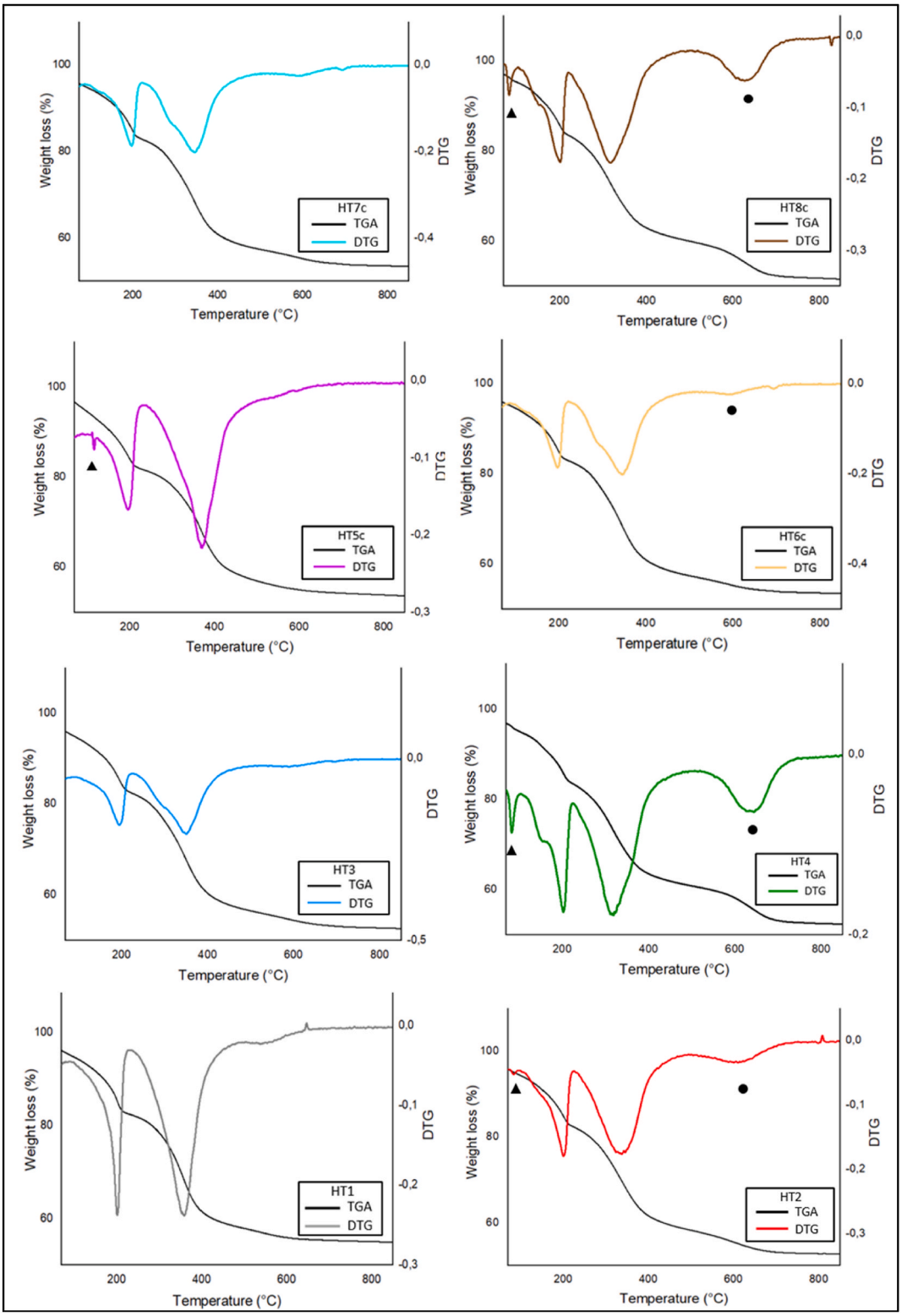

Fig. 7. Thermal analysis.

Table 6
Mass losses of the main endothermic bands (%).

LDH	Process variables	1st region of mass loss (%)	2nd region of mass loss (%)
HT1	200 rpm/2h	17.77	24.14
HT2	1000 rpm/2h	12.1	23.74
HT3	200 rpm/18h	13.39	24.83
HT4	1000 rpm/18h	11.52	22.39
HT5c	200 rpm/2h/baffle	11.03	24.55
HT6c	1000 rpm/2h/baffle	17.19	24.67
HT7c	200 rpm/18h/baffle	17.27	24.51
HT8c	1000 rpm/18h/baffle	11.53	21.71

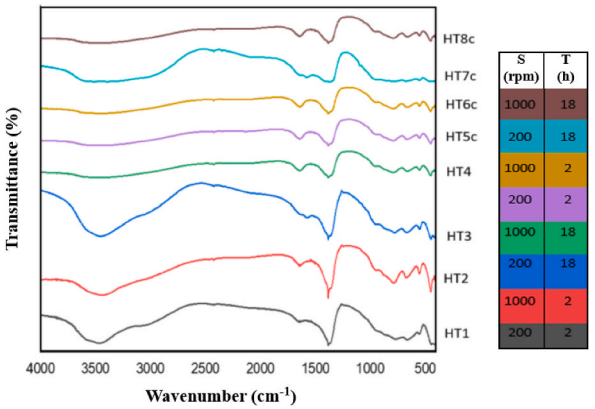

Fig. 8. FT-IR plots for the synthesized materials.

mass loss percentages from the dehydroxylation/decarbonation steps, provided in Table 6, also support these results.

Table 7 presents the adsorption/desorption isotherms for the synthesized LDHs. The areas of LDHs were obtained by the Brunauer–Emmett–Teller (BET) methodology and the distribution and pore size were obtained by the Barret-Joyner-Halenda (BJH) model. The tabulated data demonstrated that, according to the International Union of Pure and Applied Chemistry (IUPAC), all particles produced are mesoporous as they have pore diameters between 2 and 50 nm. However, the particles demonstrated differences between them, which varied with the operating conditions used. The surface areas of the materials produced varied in a range of 69.81–97.62 m^2/g, while the volumes varied in a range of 0.28–0.59 cm^3/g and the diameters of 11.40–34.66 nm.

The pore volume and pore diameter were smaller in the tests that used a lower agitation speed (HT1, HT3 and HT5c), with the exception of the HT7c test. This may be associated with the inefficiency of the mixing process as noted by the agglomerated reagent mass after completion of the total synthesis time of the tests conducted at 200 rpm (Fig. 5). In the specific case of the HT7c experiment, it is suggested that the longer aging time and the presence of baffles mitigated the effects of the low agitation speed and produced a material with improved pore volume and diameter.

As for surface area, the lowest values were 69.81 m^2/g (without baffle) and 72.67 m^2/g (with baffle) obtained in tests conducted at the highest planning levels, speed equal to 1000 rpm and time aging equal to 18 h. The HT7c material, produced at 200 rpm and aged for 18 h, presented the largest surface area among the tests (97.62 m^2/g). These results indicate the existence of a negative correlation between rotation speed and the specific surface area of LDHs, as experiments conducted at lower rotation speeds produced materials with smaller specific surface areas. This relationship is likely explained by the contribution of other factors, such as shear stress between particles generated by higher rotation speeds, and other surface forces, which were not considered in this study.

Table 7
Surface area, volume, and pore diameter of LDHs from N_2 physisorption studies.

LDH	Process variables	Surface area (m^2/g)	Pore volume (cm^3/g)	Pore diameter (nm)
HT1	200 rpm/2h	87.09	0.43	18.08
HT2	1000 rpm/2h	82.04	0.52	24.42
HT3	200 rpm/18h	76.92	0.37	17.93
HT4	1000 rpm/18h	69.81	0.58	34.66
HT5c	200 rpm/2h/baffle	89.06	0.28	11.40
HT6c	1000 rpm/2h/baffle	88.89	0.59	25.52
HT7c	200 rpm/18h/baffle	97.62	0.56	21.61
HT8c	1000 rpm/18h/baffle	72.67	0.57	33.77

3.4. Analysis of the influence of speed per image capture

The stirring speed was the variable with the greatest significance among the factors analyzed. To expand the study of the effect of this variable, an image capture study was carried out dividing the speed range, which now included the speed of 600 rpm, aiming to provide greater detail on the influence of speed on the mixing process. Thus, for image capture studies, stirring speeds of 200, 600 and 1000 rpm were used.

Fig. 9 demonstrates the treatment of the 11 frames generated from the videos recorded from the test conducted at 200 rpm. Using ImageJ software, each original frame (Fig. 9a) was converted to 8-bit grayscale images (Fig. 9b) and had the contrast altered to highlight the differences between homogeneous and non-homogeneous zones (Fig. 1c). Regions of interest (RoI) were then created (Fig. 9d), which would be the equivalent of sample points.

In each RoI, two variables were computed, the average of the pixel's gray value and the standard deviation of the pixel's gray value, which were used to calculate a third variable, the coefficient of variation (CV). For each stirring speed, these values were averaged between the replicates, obtaining a characteristic frame for each speed. Then, the mean and standard deviation of the CV between the RoIs of each characteristic condition were calculated. The CV values are shown in Table 8.

The physical significance of CV for this study is related to the homogeneity of the reaction medium, considering the set of data analyzed. The relationship that is established is that the lower the CV (data variability), the greater the homogeneity of the mixture. According to the tabulated data, the CV is lower in tests conducted at 600 and 1000 rpm. For comparative purposes, tests 2 and 3 are more homogeneous than test 1, conducted at 200 rpm. It can also be seen that the CV value varies by around 53 % between 200 rpm and 600 rpm, while between 600 rpm and 1000 rpm the variation is within the limits of the standard deviation, which indicates that they are statistically equivalent. This implies that there is no effective difference in homogeneity between tests 2 and 3 and operating between 600 and 1000 rpm is equivalent for the mixing effect.

It is also worth noting that in the literature, it is usually assumed that the system is considered homogeneous when CV is equal to or less than 5 % [46]. However, depending on the application, this limit value can vary widely and must be analyzed together with the data obtained. In this study, it was demonstrated that the tests conducted at 200 rpm presented a non-uniform final appearance, with the formation of a granular-looking gel (Fig. 5). It is then assumed that the tests conducted at 200 rpm did not result in homogeneous mixtures.

3.5. Critical analysis of results

The results demonstrated that there are significant correlations between the process variables and the formation of LDHs, and that the selection of variables, improvements in the quality of the mixtures and flow characteristics are fundamental to avoid stagnant zones, regions of low homogeneity and increased time of process.

In general, agitation speed favored the homogenization of the medium, influencing the flow characteristics of the mixture and the uniformity of the LDHs formed (Figs. 3 and 5). High speed also influenced the structural characteristics of the material; larger and more crystalline particles were produced in tests conducted at 1000 rpm (tests HT2, HT4, HT6c, and HT8c). Additionally, a positive relationship between speed and pore diameter and volume of the materials was observed.

The positive influence on the stirring speed in the LDH production process was confirmed through factorial experimental design 2^3, which demonstrated that the amount of LDH produced increases with speed (Table 3). Thus, it is possible to establish a positive relationship between the quality and the quantity of LDH produced. In general, LDHs produced in larger quantities showed better crystallinity, volume and pore size characteristics. And these characteristics were achieved by increasing the rotation speed and consequently reducing the heterogeneity of the reaction medium. Therefore, data analysis allows us to establish an increasing correlation between these three axes: homogeneity, quantity of LDH produced and crystallinity and porosity characteristics.

However, image tests demonstrated that there is a speed increase limit (Table 8), as changing the speed from 600 to 1000 rpm did not cause significant changes in terms of homogeneity of the mixture/system. Therefore, operating at the highest speed does not bring advantages in homogenizing the reactive medium and using a speed of 600 rpm would be sufficient to make the medium homogeneous. The data also allows us to infer that high speeds can cause material rupture, as attributed to tests 2 and 4, which showed a decreasing relationship between speed and the amount of LDH produced in tests produced without baffles, different from the other tests that showed a relationship increasing (Table 3). It is believed that the absence of baffles increased the shear stress between the particles, which may have caused their disintegration and impacted the definition of their structural characteristics, such as the specific surface area, which was lower in the tests conducted at 1000 rpm.

Regarding aging time, the tests demonstrated that LDH gels with greater apparent viscosity (Fig. 4) and good crystallinity (Fig. 6) were produced in tests with longer times, which demonstrates better structural organization. The factorial design also confirmed the benefit of aging time and its importance for the mixing process, demonstrating an increasing relationship between aging time and the amount of LDH produced. However, speed was in fact the most significant variable in this study.

Regarding the use of baffles, the experimental design did not indicate it as a significant variable. However, in observations regarding the appearance of the mixture, it is clear that the use of baffles contributed to the homogeneity of the system in the precipitation stage since their use promoted the rapid dilution of the basic solution (Fig. 3). However, it is suggested that this effect does not continue in the aging stage, and therefore, the factorial design did not validate the absence/presence of baffles as a significant factor.

In general, according to the analysis of Tables 3 and it is evident that the physical characteristics of the product were changed due to the process variables, which briefly presented the main information about the behavior and quantitative and qualitative characteristics

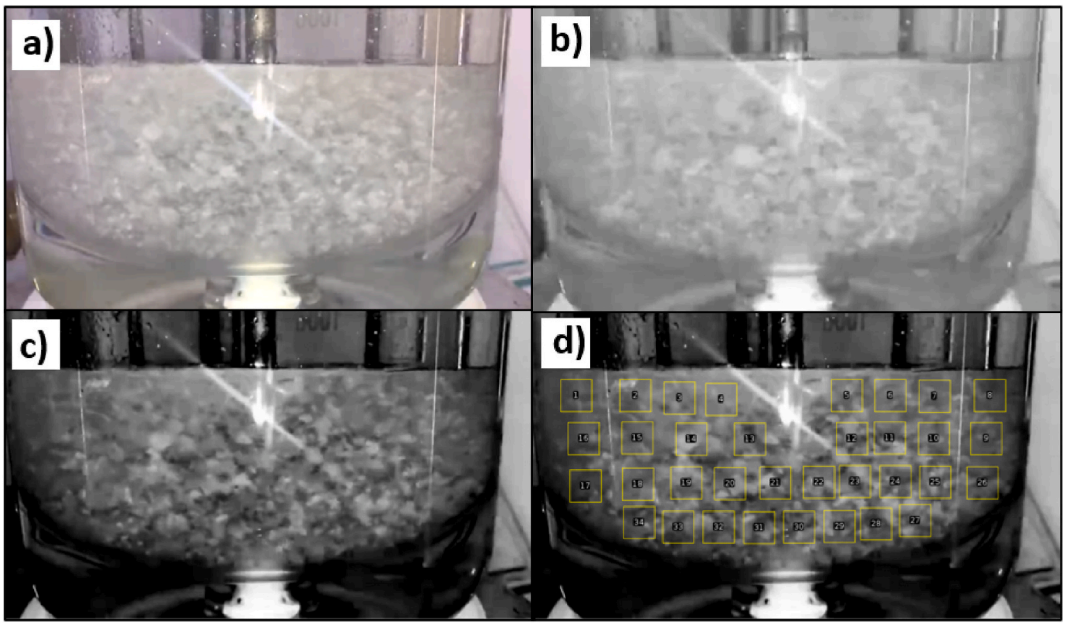

Fig. 9. Treatment of frames - a) Original, b) In 8-bit grayscale, c) With accentuated contrast and d) Positioning of the RoIs.

Table 8
Coefficient of variation (CV) values.

LDH	Stirring speed (rpm)	CV (%)
1	200.00	5.38 ± 1.18
2	600.00	2.51 ± 0.48
3	1000.00	2.69 ± 0.84

of the production of LDHs. It is worth noting that the data analyzed are valid for the study range applied 2^3 factorial design of experiment and that the objective of the design was to identify the significant variables that effectively contributed to better homogenization of the reaction system and impacted the structural characteristics of the material produced.

4. Conclusion

This study investigated the production process of Lamellar Double Hydroxides (LDHs): MgAl-LDH. Data analysis, which encompassed quantitative and qualitative results, in addition to characterizations, demonstrated that the process variables act effectively in defining the homogeneity of the mixtures. The results demonstrated the presence of a propagation effect, which initiates from the stirring tank during the production of LDHs and replicates onto the structural and chemical characteristics of the produced material. Significant differences in the homogeneity and dispersion of the reagents were observed, which caused variations in the aspects of the mixtures and in the characteristics of the LDHs, such as variations in viscosity (apparent), variations in the sedimentation and crushing processes of the materials, and in the amount of LDH produced. The result of the experimental design to evaluate the amount of LDH produced indicated that the significant factors to produce LDHs were agitation speed and aging time. The characterizations underwent significant modifications with the change in process variables. Variations in surface area data (69.81–97.62 m^2/g), pore volume (0.28–0.59 cm^3/g) and pore diameter (11.40–34.66 nm) were observed. In the FT-IR and TGA/DTG analyses, despite the obvious differences between the materials analyzed, it was not possible to establish a direct relationship between these indicators and the factors. Unlike XRD, which confirmed that the control of these variables is crucial for defining the crystallinity and particles size (70.99–174.79 nm) of the LDH produced, with the best results being obtained when the LDHs were produced at high rates of speed (1000 rpm) and longer aging times (18 h). Thus, it is evident that the study and selection of process variables in stirred tanks are fundamental in the process of transferring mass, heat and energy associated with the physical and chemical transformations that occur during their operation.

CRediT authorship contribution statement

Rafaela Gabriel: Writing – review & editing, Writing – original draft, Visualization, Methodology, Formal analysis, Data curation, Conceptualization. **Pollyanna Vanessa dos Santos Lins:** Writing – review & editing, Writing – original draft, Visualization, Formal

analysis. **Felipe de Alcântara Moura Vilela:** Writing – review & editing, Visualization, Investigation. **Sandra Helena Vieira de Carvalho:** Writing – review & editing, Resources, Investigation. **Rodolfo Junqueira Brandão:** Writing – review & editing, Writing – original draft, Visualization, Investigation. **Joao Inacio Soletti:** Writing – review & editing, Supervision, Investigation, Conceptualization. **Lucas Meili:** Writing – review & editing, Writing – original draft, Supervision, Resources, Investigation, Funding acquisition.

Declaration of competing interest

The authors declare the following financial interests/personal relationships which may be considered as potential competing interests:I am an associated editor of Heliyon – Chemical Engineering section.

Acknowledgement

The authors thank the National Council for Scientific and Technological Development (CNPq/Brazil), Coordination for the Improvement of Higher Education Personnel (CAPES/Brazil), the Brazilian Innovation Agency (FINEP), and Foundation for Research Support of the State of Alagoas (FAPEAL/Brazil).

References

[1] R. Gabriel, S. H. V. de Carvalho, J.L. da S. Duarte, L.M.T.M. Oliveira, D.A. Giannakoudakis, K.S. Triantafyllidis, J.I. Soletti, L. Meili, Mixed metal oxides derived from layered double hydroxide as catalysts for biodiesel production, Appl. Catal. Gen. 630 (2022), https://doi.org/10.1016/j.apcata.2021.118470. Elsevier B.V.
[2] S. Soulé, P. Durand, S. El-Kirat-Chatel, F. Quilès, C. Carteret, Structural features and dynamic behaviour of the interlayer space of layered double hydroxide coatings, Mater. Today Chem. 35 (2024), https://doi.org/10.1016/j.mtchem.2024.101897.
[3] Y. Tan, H. Yi, X. Tang, Q. Yu, F. Gao, J. Liu, Y. Wang, Y. Zhou, D. Kang, S. Zhao, Layered double hydroxides for air pollution control: Applications, mechanisms and trends, J. Clean. Prod. 436 (2024), https://doi.org/10.1016/j.jclepro.2024.140635. Elsevier Ltd.
[4] P.V. dos Santos Lins, D.C. Henrique, A.H. Ide, C.L. de Paiva e Silva Zanta, L. Meili, Evaluation of caffeine adsorption by MgAl-LDH/biochar composite, Environ. Sci. Pollut. Control Ser. 26 (31) (2019) 31804–31811, https://doi.org/10.1007/s11356-019-06288-3.
[5] R. Gabriel, S. H. V. de Carvalho, J.L. da S. Duarte, L.M.T.M. Oliveira, D.A. Giannakoudakis, K.S. Triantafyllidis, J.I. Soletti, L. Meili, Mixed metal oxides derived from layered double hydroxide as catalysts for biodiesel production, Appl. Catal. Gen. 630 (2022), https://doi.org/10.1016/j.apcata.2021.118470. Elsevier B.V.
[6] A. F. da Silva, J.L. da S. Duarte, L. Meili, Different routes for MgFe/LDH synthesis and application to remove pollutants of emerging concern, Separ. Purif. Technol. 264 (2021), https://doi.org/10.1016/j.seppur.2021.118353.
[7] D. Gu, C. Li, X. Gu, J. Wang, Solid-liquid mixing characteristics in a fractal cut impeller stirred reactor with dense solid loading, Chemical Engineering and Processing - Process Intensification 196 (2024), https://doi.org/10.1016/j.cep.2023.109655.
[8] A.S. Peiter, P.V.S. Lins, L. Meili, J.I. Soletti, S.H.V. Carvalho, W.R.O. Pimentel, S.M.P. Meneghetti, Stirring and mixing in ethylic biodiesel production, J. King Saud Univ. Sci. 32 (1) (2020) 54–59, https://doi.org/10.1016/j.jksus.2018.01.010.
[9] X. Yan, W. Wang, H. Zhang, D. Li, Z. Sun, H. Yang, Enhancement of liquid-solid mixing and particle hydrophobization by an impeller-less flotation pulp conditioning device, Miner. Eng. 190 (2022), https://doi.org/10.1016/j.mineng.2022.107933.
[10] A.A.A. Ahmed, Z.A. Talib, M.Z. Bin Hussein, A. Zakaria, Zn-Al layered double hydroxide prepared at different molar ratios: preparation, characterization, optical and dielectric properties, J. Solid State Chem. 191 (2012) 271–278, https://doi.org/10.1016/j.jssc.2012.03.013.
[11] A. Elhalil, M. Farnane, A. Machrouhi, F.Z. Mahjoubi, R. Elmoubarki, H. Tounsadi, M. Abdennouri, N. Barka, Effects of molar ratio and calcination temperature on the adsorption performance of Zn/Al layered double hydroxide nanoparticles in the removal of pharmaceutical pollutants, J. Sci.: Advanced Materials and Devices 3 (2) (2018) 188–195, https://doi.org/10.1016/j.jsamd.2018.03.005.
[12] J.S. Valente, H. Pfeiffer, E. Lima, J. Prince, J. Flores, Cyanoethylation of alcohols by activated Mg-Al layered double hydroxides: influence of rehydration conditions and Mg/Al molar ratio on Brönsted basicity, J. Catal. 279 (1) (2011) 196–204, https://doi.org/10.1016/j.jcat.2011.01.018.
[13] Y. Yuan, X. Zhang, Y. Lei, Y. Jiang, Z. Xu, S. Zhang, J. Gao, S. Zhao, Nitrogen removal by modified zeolites coated with Zn-layered double hydroxides (Zn-LDHs) prepared at different molar ratios, J. Taiwan Inst. Chem. Eng. 87 (2018) 73–82, https://doi.org/10.1016/j.jtice.2018.03.010.
[14] K. Zou, H. Zhang, X. Duan, Studies on the formation of 5-aminosalicylate intercalated Zn-Al layered double hydroxides as a function of Zn/Al molar ratios and synthesis routes, Chem. Eng. Sci. 62 (7) (2007) 2022–2031, https://doi.org/10.1016/j.ces.2006.12.041.
[15] N. Spogis, J.R. Nunhez, Design of a high-efficiency hydrofoil through the use of computational fluid dynamics and multiobjective optimization, AIChE J. 55 (7) (2009) 1723–1735, https://doi.org/10.1002/aic.11804.
[16] X. Sun, E. Neuperger, S.K. Dey, Insights into the synthesis of layered double hydroxide (LDH) nanoparticles: Part 1. Optimization and controlled synthesis of chloride-intercalated LDH, J. Colloid Interface Sci. 459 (2015) 264–272, https://doi.org/10.1016/j.jcis.2015.07.073.
[17] C. Modrogan, S. Căprărescu, A.M. Dăncilă, O.D. Orbuleț, E. Vasile, V. Purcar, Mixed oxide layered double hydroxide materials: synthesis, characterization and efficient application for Mn2+ removal from synthetic wastewater, Materials 13 (18) (2020), https://doi.org/10.3390/ma13184089.
[18] T.P.F. Teixeira, S.F. Aquino, S.I. Pereira, A. Dias, Use of calcined layered double hydroxides for the removal of color and organic matter from textile effluents: kinetic, equilibrium and recycling studies, Brazilian Jounal of Chemical Engeneering 31 (1) (2014) 19–26. www.abeq.org.br/bjche.
[19] T. De Saegher, J. Lauwaert, J. Hanssen, E. Bruneel, M. Van Zele, K. Van Geem, K. De Buysser, A. Verberckmoes, Monometallic cerium layered double hydroxide supported pd-ni nanoparticles as high performance catalysts for lignin hydrogenolysis, Materials 13 (3) (2020), https://doi.org/10.3390/ma13030691.
[20] K. Cermelj, K. Ruengkajorn, J.C. Buffet, D. O'Hare, Layered double hydroxide nanosheets via solvothermal delamination, J. Energy Chem. 35 (2019) 88–94, https://doi.org/10.1016/j.jechem.2018.11.008.
[21] V. Thite, S.M. Giripunje, Chloride intercalated Zn-Al layered double hydroxide nanoparticles: novel photoluminescent colloids, Mater. Res. Express 6 (10) (2019), https://doi.org/10.1088/2053-1591/ab3c8c.
[22] M. Hájek, P. Kutálek, L. Smoláková, I. Troppová, L. Čapek, D. Kubička, J. Kocík, D.N. Thanh, Transesterification of rapeseed oil by Mg-Al mixed oxides with various Mg/Al molar ratio, Chem. Eng. J. 263 (2015) 160–167, https://doi.org/10.1016/j.cej.2014.11.006.
[23] L. Wang, Y. Dou, J. Wang, J. Han, L. Liu, M. Wei, Layer-by-layer assembly of layered double hydroxide/rubber multilayer films with excellent gas barrier property, Compos. Appl. Sci. Manuf. 102 (2017) 314–321, https://doi.org/10.1016/j.compositesa.2017.07.014.
[24] M. Di Serio, M. Ledda, M. Cozzolino, G. Minutillo, R. Tesser, E. Santacesaria, Transesterification of soybean oil to biodiesel by using heterogeneous basic catalysts, Ind. Eng. Chem. Res. 45 (9) (2006) 3009–3014, https://doi.org/10.1021/ie051402o.
[25] S. Sankaranarayanan, C.A. Antonyraj, S. Kannan, Transesterification of edible, non-edible and used cooking oils for biodiesel production using calcined layered double hydroxides as reusable base catalysts, Bioresour. Technol. 109 (2012) 57–62, https://doi.org/10.1016/j.biortech.2012.01.022.
[26] N. Bálsamo, S. Mendieta, A. Heredia, M. Crivello, Nanoclays as dispersing precursors of La and Ce oxide catalysts to produce high-valued derivatives of biodiesel by-product, Mol. Catal. 481 (2020), https://doi.org/10.1016/j.mcat.2019.01.010.
[27] P. Kuśtrowski, D. Sułkowska, L. Chmielarz, R. Dziembaj, Aldol condensation of citral and acetone over mesoporous catalysts obtained by thermal and chemical activation of magnesium-aluminum hydrotalcite-like precursors, Appl. Catal. Gen. 302 (2) (2006) 317–324, https://doi.org/10.1016/j.apcata.2006.02.003.

[28] C.N. Pérez, C.A. Pérez, C.A. Henriques, J.L.F. Monteiro, Hydrotalcites as precursors for Mg,Al-mixed oxides used as catalysts on the aldol condensation of citral with acetone, Appl. Catal. Gen. 272 (1–2) (2004) 229–240, https://doi.org/10.1016/j.apcata.2004.05.045.
[29] J.I. Di Cosimo, V.K. Díez, M. Xu, E. Iglesia, C.R. Apesteguía, Structure and surface and Catalytic properties of Mg-Al basic oxides, J. Catal. 178 (1998), 0021-9517/98.
[30] S. Dasgupta, Controlled release of ibuprofen using Mg Al LDH nano carrier, IOP Conf. Ser. Mater. Sci. Eng. 225 (1) (2017), https://doi.org/10.1088/1757-899X/225/1/012005.
[31] P. Pinthong, P. Praserthdam, B. Jongsomjit, Effect of calcination temperature on mg-al layered double hydroxides (LDH) as promising catalysts in oxidative dehydrogenation of ethanol to acetaldehyde, J. Oleo Sci. 68 (1) (2019) 95–102, https://doi.org/10.5650/jos.ess18177.
[32] P. Zhao, D. Gao, H. Zhang, B. Lyu, J. Ma, S.A. Younis, K.H. Kim, Potential Applicability of Mg/Al-layered double hydroxide (LDH) for Environmentally friendly chromium-based leather tanning, ACS Sustain. Chem. Eng. 11 (30) (2023) 11110–11122, https://doi.org/10.1021/acssuschemeng.3c01681.
[33] A.L. Patterson, The scherrer formula for I-ray particle size determination, Review 56 (1939).
[34] B.B. Neto, I.R. Scarminio, R.E. Bruns, Como Fazer Experimentos, 4° Ed., 2001.
[35] A.P. Tathod, O.M. Gazit, Fundamental insights into the nucleation and growth of Mg − Al layered double hydroxides nanoparticles at low temperature, Cryst. Growth Des. 16 (2016) 6709–6713, https://doi.org/10.1021/acs.cgd.6b01272.
[36] I. Córdova Reyes, J. Salmones, B. Zeifert, J.L. Contreras, F. Rojas, Transesterification of canola oil catalized by calcined Mg-Al hydrotalcite doped with nitratine, Chem. Eng. Sci. 119 (2014) 174–181, https://doi.org/10.1016/j.ces.2014.08.009.
[37] S.S. Santos, J.A.M. Corrêa, Síntese de hidróxidos duplos lamelares do sistema Cu , Zn , Al-CO 3 : propriedades morfológicas , estruturais e comportamento térmico (Synthesis of layered double hydroxides of the Cu , Zn , Al-CO 3 system : morphological and structural properties and th, Cerâmica 57 (2011) 274–280.
[38] W. Xie, H. Peng, L. Chen, Calcined Mg-Al hydrotalcites as solid base catalysts for methanolysis of soybean oil, J. Mol. Catal. Chem. 246 (1–2) (2006) 24–32, https://doi.org/10.1016/j.molcata.2005.10.008.
[39] C.N. Pérez, C.A. Pérez, C.A. Henriques, J.L.F. Monteiro, Hydrotalcites as precursors for Mg,Al-mixed oxides used as catalysts on the aldol condensation of citral with acetone, Appl. Catal. Gen. 272 (1–2) (2004) 229–240, https://doi.org/10.1016/j.apcata.2004.05.045.
[40] J. Wang, A.G. Kalinichev, J.E. Amonette, R.J. Kirkpatrick, Interlayer structure and dynamics of Cl-bearing hydrotalcite: far infrared spectroscopy and molecular dynamics modeling, Am. Mineral. 88 (2003) 398–409, 0003-004X/03/0203–398$05.00.
[41] J.M. Fernández, M.A. Ulibarri, F.M. Labajosb, V. Rives, The effect of iron on the crystalline phases formed upon thermal decomposition of Mg-Al-Fe hydrotalcites, J. Mater. Chem. 8 (1998) 2507–2514, https://doi.org/10.1039/A804867C.
[42] O.P. Ferreira, O.L. Alves, D.X. Gouveia, A.G. Souza Filho, J.A.C. De Paiva, J.M. Filho, Thermal decomposition and structural reconstruction effect on Mg-Fe-based hydrotalcite compounds, J. Solid State Chem. 177 (9) (2004) 3058–3069, https://doi.org/10.1016/j.jssc.2004.04.030.
[43] M. Yasaei, M. Khakbiz, E. Ghasemi, A. Zamanian, Synthesis and characterization of ZnAl-NO 3 (-CO 3) layered double hydroxide: a novel structure for intercalation and release of simvastatin, Appl. Surf. Sci. 467–468 (2019) 782–791, https://doi.org/10.1016/j.apsusc.2018.10.202.
[44] Z. Jia, J. Zhang, Z. Wang, B. Wang, L. Wang, J. Cao, Z. Tao, X. Hu, An explorative analysis of the prognostic value of lactate dehydrogenase for survival and the chemotherapeutic response in patients with advanced triple-negative breast cancer, Oncotarget 9 (12) (2018). www.impactjournals.com/oncotarget/.
[45] J. Kang, T.G. Levitskaia, S. Park, J. Kim, T. Varga, W. Um, Nanostructured MgFe and CoCr layered double hydroxides for removal and sequestration of iodine anions, Chem. Eng. J. 380 (2020), https://doi.org/10.1016/j.cej.2019.122408.
[46] K. Yang, M. Tang, D. Wang, Y. Liu, H. Wang, Y. Zhang, S. Zhang, L. Nie, Experimental study of mixing performance with the tridimensional rotational flow sieve tray under low Reynolds number, Can. J. Chem. Eng. 100 (5) (2022) 1079–1090, https://doi.org/10.1002/cjce.24215.